Effects of Microarchitecture Remodeling on Disc-Bone Interface Micromechanics in a Smoke-Exposure Rat Model

Hui Li[1], Zhangke Yang[1], Joshua Kelley[1], Tong Ye[1,2], Charles A. Reitman[2], Hai Yao[1,2], Zhaoxu Meng[1], Yongren Wu[1,2]
[1]Clemson University, Clemson, SC [2]Medical University of South Carolina, Charleston, SC
hui3@g.clemson.edu

Disclosures: Hui Li(N), Zhangke Yang(N), Joshua Kelley(N), Tong Ye(N), Charles Reitman(N), Hai Yao(N), Zhaoxu Meng(N), Yongren Wu(N)

INTRODUCTION: Low back pain has been associated with intervertebral disc (IVD) degeneration, a condition that is both a significant source of discomfort for patients and costly to treat [1]. Its symptoms are more frequent and pronounced in smokers, who often experience poor treatment outcomes and serious complications [2]. Previous in vitro and in vivo animal studies have demonstrated that harmful constituents of cigarettes can disrupt the cellular gene regulation, metabolism, and biosynthesis [3], leading to IVD degenerative remodeling. Our prior studies have further elucidated the spatiotemporal IVD remodeling pattern using a smoke exposure Sprague Dawley rat model. Notably, remodeling at the disc-bone interface (i.e., bony endplate and cartilage endplate) emerged as a key predictor of IVD degeneration, marked by cartilage calcification and structural damage to collagen fibers at the microscopic level in the interface. However, the effects of microarchitecture remodeling on disc-bone interface micromechanics remain unclear. This study aims to investigate the impact of cartilage calcification, collagen fiber angle and diameter gradient alterations on the mechanical response of the disc-bone interface using a mesoscale computational model. We hypothesize that microarchitecture remodeling compromises the mechanical integrity of the disc-bone interface, specifically the toughness and failure strain. This work contributes to a deeper understanding of IVD pathomechanics, particularly in the context of cigarette smoking.

METHODS: Twenty-four male Sprague Dawley rats, obtained with institution approval, were randomly assigned into two groups, control (n=12) and smoke exposure (n=12). Smoke exposure rats underwent daily smoking treatments daily for two months. Spinal motion segments were harvested from each group. The L4-L5 motion segment was cut sagittally and thin slices from the midplane were stained using H&E for histological analysis (**Fig.1A**). The L2-L3 and L3-L4 motion segments, prepared sagittally using a microtome to expose the midplane, were imaged using second harmonic generation (SHG) (**Fig.1B**), and scanning electron microscopy (SEM) at 400× magnification (**Fig.2A**), respectively. The mesoscale computational models consisted of a collagen fiber bundle unit with two branches, designed to mimic the disc-bone insertion. To replicate the collagen fiber structure in the annulus fibrosus (AF) region, two specific models were developed: an angular model featuring an angled collagen fiber bundle to represent the posterior AF, and a diameter gradient model incorporating a radial fiber diameter gradient to represent the anterior AF (**Fig. 2B**). Simulations were conducted for each model to predict the behavior of collagen fibers under varying conditions, including the presence or absence of cartilage calcification, as well as variations in collagen fiber bundle angle and diameter gradient. Mechanical property parameters, including maximum stress, elastic modulus, toughness, and failure strain, were calculated based on the model output of the stress-strain curve. Furthermore, mesoscale deformation and failure mechanisms, specifically the kinetic behaviors of fiber bond breakage, were investigated.

RESULTS: Mesoscale angular modeling results demonstrate that calcified collagen fibers exhibit greater maximum stress ($\sigma_{max,\,c}$ = 12.73 MPa; $\sigma_{max,\,u}$ = 5.16 MPa), greater elastic modulus E_c = 438.45 MPa, E_u = 175.99 MPa), and increased pre-failure toughness ($T_{c,\,pre}$ = 17.94 J/m^4, $T_{u,\,pre}$ = 7.26 J/m^4) compared to uncalcified collagen fibers. Furthermore, the post-failure toughness in the angular model is greater than in the non-angular model (with angle: $T_{u,\,post}$ = 4.96 J/m^4, without angle: $T_{u,\,post}$ = 0.59 J/m^4), despite a slight reduction in maximum stress, elastic modulus, and pre-failure toughness (**Fig.3A**). In the diameter gradient model, calcified collagen fibers also exhibited greater maximum stress ($\sigma_{max,\,c}$ = 7.41 MPa; $\sigma_{max,\,u}$ = 5.56 MPa), a greater elastic modulus (E_c = 415.07 MPa, E_u = 214.04 MPa), and a lower failure strain (ε_c = 1.6%, ε_u = 2.4%). Additionally, there is no significate difference in post-failure toughness between the small diameter gradient and large diameter gradient model (Small gradient: $T_{u,\,post}$ = 7.68 J/m^4, Large gradient: $T_{u,\,post}$ = 6.05 J/m^4) (**Fig.3B**).

DISCUSSION: Calcification adversely affects the mechanical properties at the disc-bone interface by increasing maximum stress but simultaneously reducing resilience, as evidenced by a decrease in failure strain and post-failure toughness compared to uncalcified conditions (**Fig.3**). This reduction in resilience heightens the risk of catastrophic failure, particularly under circumstances involving large deformations driven by stress concentration at the calcified interface. Moreover, the diameter gradient model demonstrates lower maximum stress and failure strain compared to the angular model, primarily due to the inhomogeneous stress distribution, particularly the stress concentration and collagen fiber bond breakage at the insertion in the diameter gradient model. The rotational movements of the branching structure in the angular model further facilitates more energy dissipation compared to the diameter gradient model. Although the different diameter gradient types do not show significant differences under uniform axial tensile loading, in realistic scenarios, the loading in the outer AF is greater than in the inner AF under spine flexion and extension conditions. A steeper diameter gradient with larger outer collagen fiber bundles would be more effective in minimizing stress concentration at the endplate interface, thereby providing more superior loading support capacity. In summary, a healthy disc-bone interface functions as a well-organized, cohesive structure that facilitates deformability and optimal stress distribution due to its branching architecture, which dynamically fine-tunes the mechanical performance and enables effective energy absorption under mechanical loading. However, interface calcification impairs this regulatory kinetic capacity by rendering the collagen fiber stiffer and more brittle, thereby compromising the stress distribution and contributing to propagation of collagen fiber bond breakage.

SIGNIFICANCE/CLINICAL RELEVANCE: We developed a mesoscale computational model, supported by advanced imaging techniques, to understand the detrimental effect of microarchitecture remodeling on the micromechanics of disc-bone interface. The findings suggest that collagen fiber bond-breaking events at the disc-bone insertion may contribute to integrity degradation and microfracture formation under mechanical loading. By helping to better understand the IVD pathomechanics, this research aims to establish a scientific foundation for potential earlier diagnosis and optimized treatment of IVD degeneration, with a focus on enhancing the integrity and mechanical function of the endplate interface.

REFERENCES: [1] Lyu FJ, et al. Painful intervertebral disc degeneration and inflammation. Bone Res. 2021; 9:7. [2] Rajesh N, et al. Smoking and degenerative spinal disease: a systematic review. Brain Spine. 2022; 2:100916. [3] Wang D, et al. Spine degeneration in a murine model of smokers. Osteoarthritis Cartilage. 2012;20(8):896-905.

ACKNOWLEDGEMENTS: This work was supported by NIH/NIGMS COBRE: South Carolina Translational Research Improving Musculoskeletal Health (SC TRIMH; P20GM121342), and the Cervical Spine Research Society Seed Starter Grant.

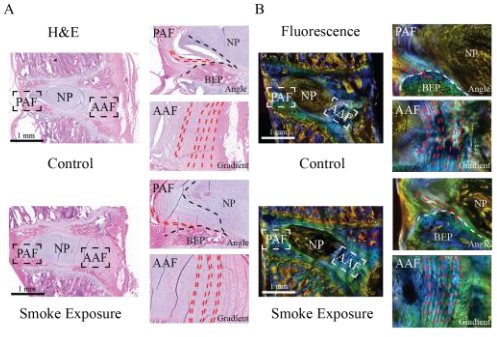

Fig. 1. Representative images of the AF region in sagittal sections from control and smoke-exposed samples, using (A) histology and (B) fluorescence.Notes: NP: nucleus pulposus; BEP: bony endplate; AAF: anterior AF; PAF: posterior AF.

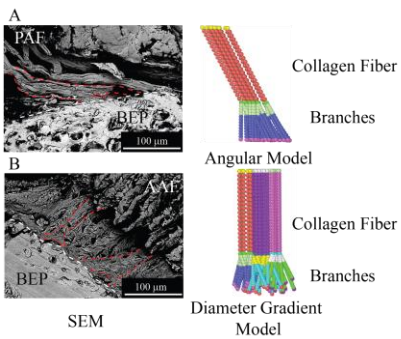

Fig. 2. Representative images and schematic illustrations of the collagen fiber structure in the AF region: (A) the angular model, and (B) the diameter gradient model.

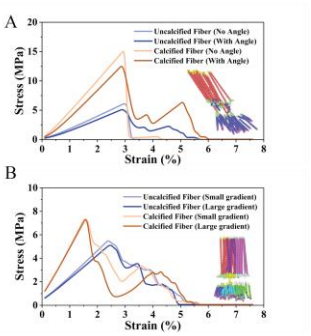

Fig. 3. Stress-strain curves in (A) the angular model and (B) the diameter gradient model.